

# Full reconstruction of acoustic wavefields by means of pointwise measurements

Denis V. Makarov, Pavel S. Petrov,

## Abstract

Sound propagation in the ocean is considered. We demonstrate a novel algorithm for full wavefield reconstruction using pointwise measurements by means of a vertical array. The algorithm is based on the so-called discrete variable representation and can be implemented both for tonal and pulse signals. It is shown that the algorithm is robust against array distortions and ambient noise of moderate amplitude. Efficiency of reconstruction is verified by means of numerical simulation with a model of a shallow-sea waveguide. It is found that the effect of bottom sound attenuation enables accurate reconstruction with arrays having relatively low density of hydrophones.

## Index Terms

underwater acoustics, vertical array, discrete variable representation, bottom attenuation

# Full reconstruction of acoustic wavefields by means of pointwise measurements

## I. INTRODUCTION

Efficient solving of various problems concerned with wave propagation often requires accurate reconstruction of a continuous wavefield relying upon data of pointwise measurements. It is of the especial importance in inverse problems where even tiny features of an interference pattern might give information about medium passed by a wave, or information about properties of a wave source. In the context of underwater acoustics, it allows for straightforward extraction of wavefield constituents corresponding to individual modes [1], [2], [3], [4], [5], rays [6], and the so-called stable components being Gaussian wavepackets with minimal uncertainty [7]. Expansion of a wavefield over individual modal contributions can be used, for example, for long-range environment reconstruction using mode-based schemes of hydroacoustical tomography [8], [9], [10], [11]. Also, detailed analysis of a wavefield structure is helpful for robust identification of propagation geometry, that is of great importance for geoacoustic inversion [12] and seismic surveys [13], [14], as well as for various kinds of the matched field processing [15], [16], [17]. Development of receiving-transmitting arrays allowing for full and accurate reconstruction is important in the context of applications associated with sound focusing, like underwater communication [4], [18] and remote monitoring of the ocean bottom [19], [20]. Detailed information about a wavefield structure facilitates experimental investigation of scattering physics [21], [22], [23], [24], [25], [26], especially in the context of wave chaos [27], [28], [29], [30], [31], [32].

Basically, the possibility of full reconstruction of a wavefield by means of a vertical array follows from the Kotelnikov-Shannon-Nyquist theorem that determines the optimal sampling rate for representation of a continuous function by means of a discrete sequence. It implies exact reconstruction of a continuous wave (CW) field with wavelength  $\lambda$  by means of a vertical array of hydrophones spaced by  $\lambda/2$ . In the present study we show that optimal spacing can significantly exceed  $\lambda/2$  due to the filtration of high-number modes. The main result of the paper is the algorithm of exact reconstruction that takes into account boundary conditions in the waveguide. The algorithm is closely related to the so-called discrete variable representation. Sensitivity of the algorithm to random fluctuations that can be caused by ambient noise or distortions of the array is also examined.

The paper is organized as follows. The next section describes the discrete variable representation technique. Reconstruction of tonal wavefields is considered in Section III. Short Section IV is devoted to array spacing values which provide accurate reconstruction. Section V is devoted to reconstruction of broadband pulses. In the Conclusion, we summarize and discuss the obtained results. Also we outline possible extensions of the algorithm and future work.

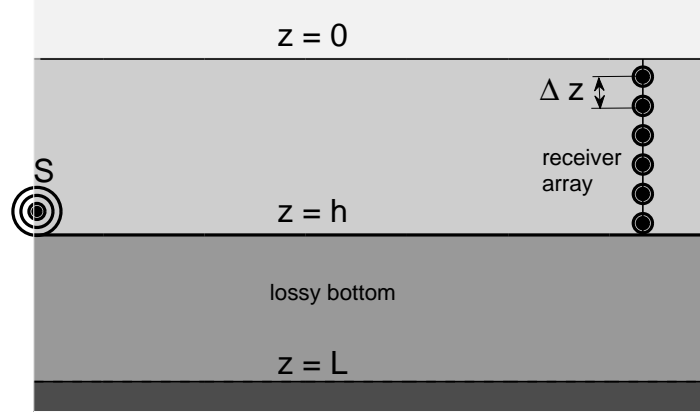


Fig. 1: A shallow-water waveguide with a sound source (S) and a vertical receiver array.

44

## II. DISCRETE VARIABLE REPRESENTATION FUNCTIONS

The Kotelnikov-Shannon-Nyquist theorem considers a continuous function  $\Psi(\tau)$  having finite bandwidth  $B$  (in Hz). The theorem states that  $\Psi(\tau)$  can be exactly reproduced by a discrete sequence of values  $\Psi(\tau = nT_B)$ , where  $T_B \leq 1/(2B)$ . The reproduction can be accomplished by the Whittaker-Shannon interpolation formula

$$\Psi(\tau) = \mu \sum_{n=-\infty}^{\infty} \Psi(\tau_n) \chi_n(\tau). \quad (1)$$

where  $\mu$  is some constant depending on the normalization condition adopted,  $\tau_n = nT_B$ ,

$$\chi_n(\tau) = \text{sinc} \left( \frac{\tau - \tau_n}{T_B} \right). \quad (2)$$

45 Here the sinc function is defined as  $\text{sinc}(x) = \sin \pi x / \pi x$ . The variable  $\tau$  can be time or spatial coordinate. The  
 46 latter case anticipates that the Kotelnikov-Shannon-Nyquist theorem can be readily implemented in wave theory.

The present work is devoted to sound propagation in an underwater waveguide. We are particularly interested in reproduction of an acoustic wavefield relying upon measurements taken by a vertical array of receivers (see Fig. 1). Thus, we seek for the wavefield presentation of the following form

$$\Psi(z) = \mu \sum_{j=1}^J \Psi(z_j) \chi_j(z). \quad (3)$$

47 Here  $z_j$  are depths of hydrophones being the array elements. As long as a waveguide is bounded in the vertical  
 48 direction, the right-hand side of Eq. (3) is finite sum.

A wavefield must satisfy the boundary conditions in a waveguide, therefore, formula (2) for  $\chi_j(z)$  is not valid for guided wave propagation in general. Acoustically soft ocean surface can be fairly modelled by the Dirichlet boundary condition

$$\Psi(z = 0) = 0. \quad (4)$$

Let us also assume that the bottom is flat and consists of two layers, a penetrable sediment and impenetrable basement. At the sediment-to-basement boundary  $z = L$  we impose Neumann boundary condition

$$\frac{d\Psi}{dz}(z = L) = 0. \quad (5)$$

Our goal is to obtain such set of functions  $\chi_j(z)$  that the wavefield reconstruction is accurately accomplished by the formula Eq. (3). It can be done using the so-called discrete variable representation theory [33] (or shortly DVR), and the resulting set of functions  $\chi_j(z)$  can be referred to as DVR functions. DVR is extensively used in quantum mechanics in the context of multidimensional and/or many-body quantum calculations [33], [34], construction of atomic Wannier states in periodic potentials [35], and excitons in quantum dots [36]. Basically, the main idea of the DVR approach is to construct a basis in which the position operator (in our case  $z$ -coordinate operator) is diagonalized.

The first step of the derivation is the introduction of an auxiliary basis formed by spatial harmonics of the following form

$$\phi_j = \sqrt{\frac{2}{L}} \sin \frac{(2j-1)\pi z}{2L}, \quad j = 1, 2, \dots \quad (6)$$

We see that this set satisfies boundary conditions (4) and (5). Function  $\Psi$  can be expanded over harmonics (6),

$$\Psi(z) = \sum_j a_j \phi_j(z).$$

Amplitudes of wavefield expansion over functions  $\phi_j$  are given by the formula

$$a_j = \int_{z=0}^L \phi_j(z) \Psi(z) dz.$$

We assume that a wavefield can be exactly reproduced using superposition of harmonics  $\phi_j$  with  $j \leq j_{\max}$ , i. e. vertical wavenumber spectrum of  $\Psi$  has finite bandwidth. Our assumption can be mathematically expressed as

$$\sum_{j=1}^{j_{\max}} |a_j|^2 = \int_{z=0}^L \Psi^*(z) \Psi(z) dz. \quad (7)$$

The parameter  $j_{\max}$  is finite for any wavefield except for the particular case  $\Psi(z) = \delta(z - z_0)$ , where  $\delta(z)$  is the delta function. Using the auxiliary basis set, we can construct the  $j_{\max} \times j_{\max}$  matrix  $\mathbf{Z}$  with the entries

$$Z_{mn} = \int_{z=0}^L \phi_m^*(z) f(z) \phi_n(z) dz. \quad (8)$$

where  $f(z)$  is a monotonic and invertible function. Generally speaking, presentation of an acoustic wavefield in the form of expansion (3) requires tridiagonal form of the matrix  $\mathbf{Z}$  [33]. It holds if

$$f = \cos \frac{\pi z}{L}, \quad 0 < z \leq L. \quad (9)$$

One can find eigenvalues and eigenvectors of the matrix  $\mathbf{Z}$  by solving the problem

$$\mathbf{Z} \vec{V}_j = f_j \vec{V}_j, \quad j = 1, 2, \dots, j_{\max}. \quad (10)$$

The DVR theory allows one to find the DVR functions using eigenvectors  $\vec{V}_j$  of the matrix  $\mathbf{Z}$ ,

$$\chi_j(z) = \sum_{i=1}^{j_{\max}} V_{ij} \phi_i(z), \quad (11)$$

where  $V_{ij}$  is the  $i$ -th entry of the  $j$ -th eigenvector  $\vec{V}_j$ . Formula (11) ensures that DVR functions obey boundary conditions (4) and (5). Eigenvectors can be found analytically:

$$V_{ij} = \sqrt{\frac{2}{j_{\max} + 1}} \sin \left[ \frac{(i - \frac{1}{2})j\pi}{j_{\max} + 1} \right]. \quad (12)$$

Functions  $\chi_j(z)$  also form complete orthogonal basis set if the condition (7) is satisfied. It means that an arbitrary wavefield satisfying (7) can be expanded over DVR functions,

$$\Psi(z) = \sum_{j=1}^{j_{\max}} b_j \chi_j(z). \quad (13)$$

The most important property of the DVR basis is the relation between amplitudes of this expansion and local values of  $\Psi(z)$  [33],

$$b_j = \sqrt{\Delta z} \Psi(z = z_j), \quad (14)$$

where depth values  $z_j$  are determined by eigenvalues of  $\mathbf{Z}$ ,

$$z_j = z(f_j). \quad (15)$$

56 The property (14) provides means for reconstruction of a wavefield by means of pointwise measurements via a  
57 vertical array of hydrophones located at depths  $z_j$ .

Eigenvalues  $f_j$  are given by a simple formula

$$f_j = \cos \left( \frac{j\pi}{j_{\max} + 1/2} \right). \quad (16)$$

They determine depths of array elements

$$z_j = z(f_j) = j\Delta z, \quad (17)$$

where  $\Delta z$  is array spacing,

$$\Delta z = \frac{L}{j_{\max} + 1}. \quad (18)$$

Thus, we see that the DVR representation using the auxiliary basis (6) corresponds to an equispaced vertical array. The array spacing is determined by the parameter  $j_{\max}$  that in turn is determined by the vertical Fourier spectrum of a wavefield. Comparing (3) with (13) and (14), we find that the constant  $\mu$  in the expansion (3) is determined by the array spacing,

$$\mu = \sqrt{\Delta z}. \quad (19)$$

So, the formula (3) becomes

$$\Psi(z) = \sqrt{\Delta z} \sum_{j=1}^J \Psi(j\Delta z) \chi_j(z). \quad (20)$$

This formula allows one to reconstruct a continuous profile of an acoustic field by means of pointwise measurements using a vertical array, if condition (7) is satisfied. Accuracy of reconstruction depends on how exactly the condition (7) is fulfilled. It can be quantified as

$$\epsilon = \left| \sum_{j=1}^{j_{\max}} |a_j|^2 - \int_{z=0}^L \Psi^*(z)\Psi(z) dz \right|. \quad (21)$$

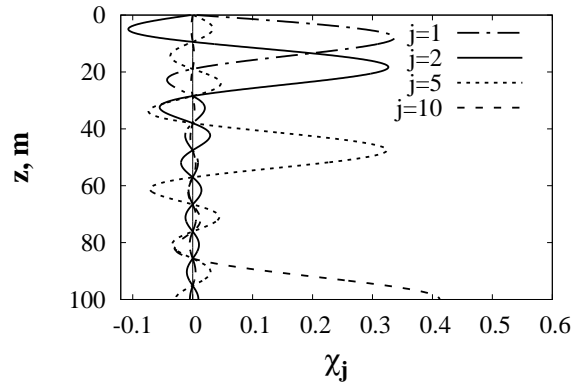


Fig. 2: DVR functions corresponding to  $j_{\max} = 10$  for a waveguide with  $L = 100$  meters. The corresponding depth eigenvalues are 9.52 meters for  $j = 1$ , 19.04 meters for  $j = 2$ , 47.62 meters for  $j = 5$ , and 95.24 meters for  $j = 10$ .

58

59 In Fig. 2 several DVR functions corresponding to  $j_{\max} = 10$  are presented. It is clear that each DVR function  
 60 is localized in a vicinity of the corresponding depth eigenvalue. All DVR functions obey the boundary conditions  
 61 given by Eqs. (4) and (5).

Number of hydrophones needed for the full reconstruction of a vertical wavefield profile decreases with decreasing  
 of  $j_{\max}$ . On the other hand, limitations on a wavefield structure imposed by Eq. (7) also become more significant  
 as  $j_{\max}$  decreases. It means that there should be some optimal value of  $j_{\max}$  that combines technical simplicity of  
 the array with high quality of reconstruction. As was mentioned before, in an unbounded isovelocity medium the  
 optimal spacing value is given by the the Kotelnikov-Shannon-Nyquist theorem as

$$\Delta z_{\infty} = \frac{\lambda}{2}. \quad (22)$$

62 However, typical underwater acoustical environment must be considered as a bounded vertically-stratified waveguide  
 63 rather than an unbounded medium, since they are often approximately homogeneous only in the horizontal directions.  
 64 It is known that in such layered media field components with large vertical wavenumbers are strongly attenuated  
 65 in course of sound propagation due to the interaction with the seabottom [37]. This effect can be also explained by  
 66 ray escaping as considered in [38], [39]. It can be therefore anticipated that the optimal value of the array spacing  
 67 can significantly exceed  $\Delta z_{\infty}$ .

It is worthwhile to mention that Eq. (20) remains valid if we consider real-valued sound pressure field  $u = \text{Re}\Psi$  instead of a complex-valued wavefield  $\Psi$ . Then Eq. (20) reads

$$u(z) = \text{Re} \left( \sum_{j=1}^{j_{\max}} b_j \chi_j(z) \right). \quad (23)$$

68 Note that strictly speaking the truncated representation of the wavefield Eq. (3) (consisting of the first  $J$  terms) is  
 69 an approximation. Thus, the DVR functions constructed above in fact form a basis in a finite-dimensional subspace  
 70 of the space of square-integrable functions on the interval  $[0, L]$ , and the functions  $\chi_j(z)$  are associated with the  
 71 restriction of the position operator to this subspace [33]. As shown in the examples below, the inaccuracy arising  
 72 from this simplification does not substantially affect the accuracy of the wavefield reconstruction.

73 It might seem more natural to start the construction of the DVR functions with the basis  $\phi_j(z)$  consisting of  
 74 normal modes. However, it is essential for the DVR approach that matrix  $\mathbf{Z}$  is tridiagonal, and it is unclear how to  
 75 ensure this property for the normal modes in general case (i.e., how to choose the function  $f(z)$  for a given sound  
 76 speed profile and bottom properties in such a way that  $\mathbf{Z}$  is tridiagonal).

### 77 III. RECONSTRUCTION OF TIME-HARMONIC WAVEFIELDS

#### 78 A. Model of a waveguide

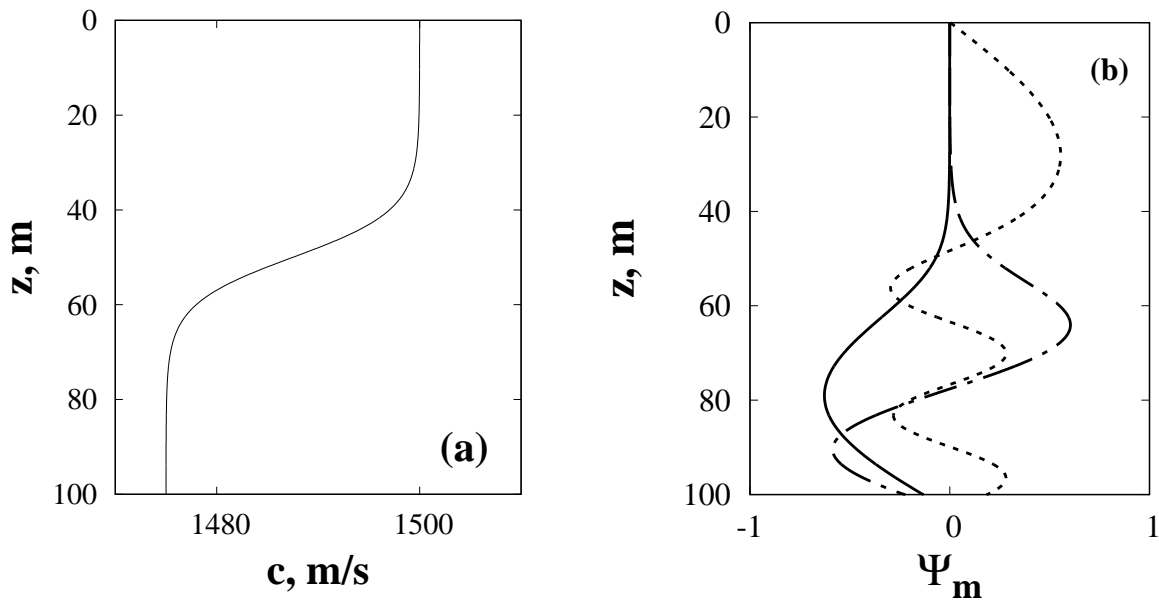


Fig. 3: (a) Sound speed profile. (b) Profiles of the first (solid line), second (dash-dotted line), and fifth (dashed line) normal modes for frequency 300 Hz.

In this section we perform numerical validation of the accuracy of wavefield reconstruction using Eq. (20) in the case of cw signals. For numerical simulation, we use a model of a shallow-water waveguide with the sound-speed

profile described by formula

$$c(z) = \begin{cases} c_0 - \frac{\Delta_c}{2} \left[ 1 + \tanh \left( \frac{z - z_c}{\Delta_z} \right) \right], & 0 \leq z < h, \\ c_b, & h \leq z \leq L, \end{cases} \quad (24)$$

79 where  $c_0 = 1500$  m/s is sound speed at the ocean surface,  $\Delta_c = 25$  m/s,  $z_c = 50$  m,  $\Delta_z = 10$  m,  $c_b = 1600$  m/s,  
 80  $L = 300$  m. The interface at the depth  $z = h = 100$  m separates the water and sediment layers. The profile is  
 81 presented in Fig. 3(a). Waves propagating in this waveguide can be conditionally divided into two classes. The first  
 82 class corresponds to the waves that propagate inside the near-bottom waveguide and do not reach the surface due to  
 83 the refraction inside the water volume (more precisely, in the layer with sound speed gradient, or the thermocline).  
 84 The waves that propagate in the whole water volume and experience reflections from both natural boundaries, i.e.  
 85 from the bottom and the surface, belong to the second class. These two classes of waves are called reflected-refracted  
 86 and reflected-reflected, respectively [37].

Acoustical field in this shallow-water waveguide satisfies the 2D Helmholtz equation

$$\frac{\partial^2 \Psi}{\partial r^2} + \frac{1}{r} \frac{\partial \Psi}{\partial r} + \rho \frac{\partial}{\partial z} \left[ \rho \frac{\partial \Psi}{\partial z} \right] + k_0^2 n^2 \Psi = 0, \quad (25)$$

where  $r$  is range,  $\rho(z)$  is the density profile in the considered cross-section of the waveguide,  $k_0 = 2\pi f/c_{\min}$ , is  
 the reference wavenumber,  $c_{\min} = c_0 - \Delta_c$  is the minimal sound speed in a water column, and  $f$  is the sound  
 frequency. Refractive index  $n(z)$  is given by formula

$$n(z) = \frac{c_0}{c(z)} + 2i\alpha(f)\Theta(z - h), \quad (26)$$

where  $\Theta(z - h)$  is the Heaviside function,  $\alpha = 0.42 \times 10^{-6} f^2$  dB/m. The imaginary term describes sound attenuation  
 in the sediment. The density profile is given by the step function

$$\rho(z) = \begin{cases} \rho_{\text{wat}}, & 0 \leq z \leq h, \\ \rho_{\text{sed}}, & h \leq z \leq L, \end{cases} \quad (27)$$

87 where  $\rho_{\text{wat}} = 1$  g/cm<sup>3</sup>,  $\rho_{\text{sed}} = 1.7$  g/cm<sup>3</sup>. The sediment parameters correspond to conditions of the East China Sea  
 88 [40].

Consider a wavefield emitted by a point source located at the depth  $z = z_s$ . Invoking the far-field approximation,  
 we can express the wavefield as superposition of normal modes of the form

$$\begin{aligned} \Psi(r, z) &= \frac{i}{2\sqrt{2\pi r}} e^{-i\pi/4} \times \\ &\times \sum_{m=1}^M \frac{1}{\sqrt{k_{rm}}} e^{i(k_{rm} + i\alpha_m)r} \Psi_m(z_s) \Psi_m(z), \end{aligned} \quad (28)$$

where  $\Psi_m(z)$  is the eigenfunction of the  $m$ -th normal mode,  $M$  is number of normal modes belonging to the  
 discrete spectrum (often called waterborne modes),  $k_{rm}$  and  $\alpha_m$  are horizontal wavenumber and attenuation rate  
 of the  $m$ -th normal mode, respectively, and ‘‘c. c.’’ means complex conjugation. Normal modes are solutions of the  
 Sturm-Liouville problem [37]

$$\rho(z) \frac{d}{dz} \left[ \frac{1}{\rho(z)} \frac{d\Psi_m(z)}{dz} \right] + [k_0^2 n^2(z) - k_{rm}^2] \Psi_m(z) = 0, \quad (29)$$



with the boundary conditions

$$\Psi(0) = 0, \quad \left. \frac{d\Psi}{dz} \right|_{z=L} = 0 \quad (30)$$

and usual continuity conditions for the modal function [37]

$$\begin{aligned} \Psi|_{z=L-0} &= \Psi|_{z=L+0}, \\ \frac{1}{\rho_{\text{wat}}} \left. \frac{d\Psi}{dz} \right|_{z=L-0} &= \frac{1}{\rho_{\text{sed}}} \left. \frac{d\Psi}{dz} \right|_{z=L+0}, \end{aligned} \quad (31)$$

89 at the water-sediment interface  $z = h$ . In the next paragraph we compare wavefields modelled using Eq. (28) with  
 90 their reconstructed counterparts. In all examples considered below Sturm-Liouville problem (29) was solved using  
 91 the code `ac_modes` [41] developed by the authors.

## 92 B. Reconstruction in the noiseless environment

Accuracy of reconstruction is quantified using the fidelity defined as [42]

$$F = \frac{1}{A_{\text{exact}} A_{\text{est}}} \left| \int_{z=0}^h \Psi_{\text{exact}}^*(z) \Psi_{\text{est}}(z) dz \right|^2, \quad (32)$$

where  $\Psi_{\text{exact}}(z)$  is a modelled wavefield considered as an “exact” solution, and  $\Psi_{\text{est}}(z)$  is a result of reconstruction using Eq. (23). The normalization factors  $A$  and  $A_{\text{est}}$  are  $L^2[0, h]$ -norms of modelled and reconstructed wavefields, respectively,

$$A_{\text{exact}} = \int_{z=0}^h |\Psi_{\text{exact}}(z)|^2 dz, \quad A_{\text{est}} = \int_{z=0}^h |\Psi_{\text{est}}(z)|^2 dz.$$

According to the definition (32),  $F = 1$  if the modelled and reconstructed wavefields coincide, and tends to zero as differences between them grow. The upper limit of integration in Eq. (32) is taken of  $h$ , i. e. the depth of water-sediment interface. It means that we assume that a vertical array spans only the water layer, and the acoustical field inside the sediment is not taken into account for the fidelity calculation. Then number of hydrophones in the array is given by the formula

$$J = \text{floor} \left( j_{\text{max}} \frac{h}{L} \right), \quad (33)$$

93 where  $\text{floor}(x)$  is the function that produces rounding down of  $x$  if  $x$  is not integer.

In the present section we consider only cw wavefields. Reconstruction of broadband pulses will be considered in Sec. V. We consider wavefields created by a point source located near the bottom, at  $z = 99$  m, at various ranges. One can conditionally define confidence range of an array in the frequency space as a sufficiently broad frequency interval where

$$F > 0.9. \quad (34)$$

94 Figs. 4(a)-(c) demonstrate the dependence of fidelity on the signal frequency for the array consisting of 10  
 95 hydrophones, i. e. for  $j_{\text{max}} = 30$ . The corresponding receiver spacing in the array is 9.52 m. We see that width of  
 96 the frequency confidence range strongly depends on distance. In the case of  $r = 1$  km, the array provides accurate  
 97 reconstruction of a wavefield for frequencies up to 80 Hz. It is very close to the critical frequency predicted by the

98 Kotelnikov-Shannon-Nyquist theorem that is equal to 75 Hz. Increasing of distance results in the suppression of of  
 99 high-number modes due to the bottom attenuation, and therefore, scale of vertical interference pattern significantly  
 100 increases. It remarkably expands the confidence range: its upper boundary is 220 Hz for  $r = 10$  km, and 260 Hz  
 101 for  $r = 40$  km.

102 Decreasing of array spacing enhances its capability to resolve fine-scale features of the interference pattern and  
 103 leads to significant broadening of the confidence range (see Figs. 4(d)-(f) and 4(g)-(i)). In the case of the array  
 104 with 15 hydrophones, the upper boundary of the confidence range is 330 Hz for  $r = 10$  km, and 490 Hz for  
 105  $r = 40$  km. Data for  $r = 1$  km presented in Fig. 4(d) deserves particular attention: frequency dependence of fidelity  
 106 is surprisingly non-monotonic, and there is an interval of lowered fidelity in the middle of the confidence range,  
 107 near  $f \simeq 145$  Hz. This kind of non-monotonicity is associated with the competition of two factors: decreasing of  
 108 wavelength that results in the reconstruction quality deterioration, and growth of sound attenuation that facilitates  
 109 suppression of high-number modes. The latter factor tends to restore fidelity with increasing frequency, as shown  
 110 in Fig. 4(d).

111 Strictly speaking, the data presented in Fig. 4(d) exhibits pointwise violation of inequality (34) at  $f = 144.4$  Hz,  
 112 where  $F = 0.88$ , but we consider it as non-essential. A more pronounced example of the fidelity non-monotonicity  
 113 in the low-frequency range is presented in Fig. 5(a), where lowering of fidelity leads to splitting of the confidence  
 114 range into two parts.

115 The array with 20 hydrophones provides broad confidence range for all considered distances. The upper boundary  
 116 is 410 Hz for  $r = 1$  km, 450 Hz for  $r = 10$  km, and 740 Hz for  $r = 40$  km.

117 Distribution of acoustical energy over modes depends on the source position. Placing the source closer to the  
 118 ocean surface, we can enhance impact of high-number modes and reduce their filtering. It worsens quality of  
 119 reconstruction and diminishes fidelity values. Figure 5 represents fidelity dependence on frequency for the array  
 120 with 20 hydrophones and the point source located near the surface, at  $z = 1$  m. We see that width of the frequency  
 121 confidence range is diminished as compared with data presented in Fig. 4(g)-(i). In addition, the confidence range  
 122 in the case of  $r = 1$  km is divided into two parts. It is a manifestation of the aforementioned effect of fidelity  
 123 non-monotonicity associated with enhanced mode filtration for high frequencies.

### 124 C. Impact of noise and fluctuations

It is reasonable to examine sensitivity of the reconstruction to ambient noise and inaccuracies in hydrophone  
 positioning. Effect of noise can be modelled as random perturbation  $\xi_j$  of measured values of acoustic pressure,

$$\Psi_{\text{measured}}(z_j) = \Psi(z_j) + \xi_j. \quad (35)$$

125 We considered several models of ambient noise. The most significant destructive effect onto accuracy of recon-  
 126 struction comes from spatially white noise, when values of  $\xi_j$  with different  $j$  are uncorrelated, and their variances  
 127 don't depend on  $j$ . Models of noise generated by the ocean surface affect reconstruction to smaller extent. As  
 128 long as we are interested in testing reliability of reconstruction under the noise disturbances, it is reasonable to  
 129 consider the most worse case. Therefore, we present below the results obtained with spatially white noise. Taking

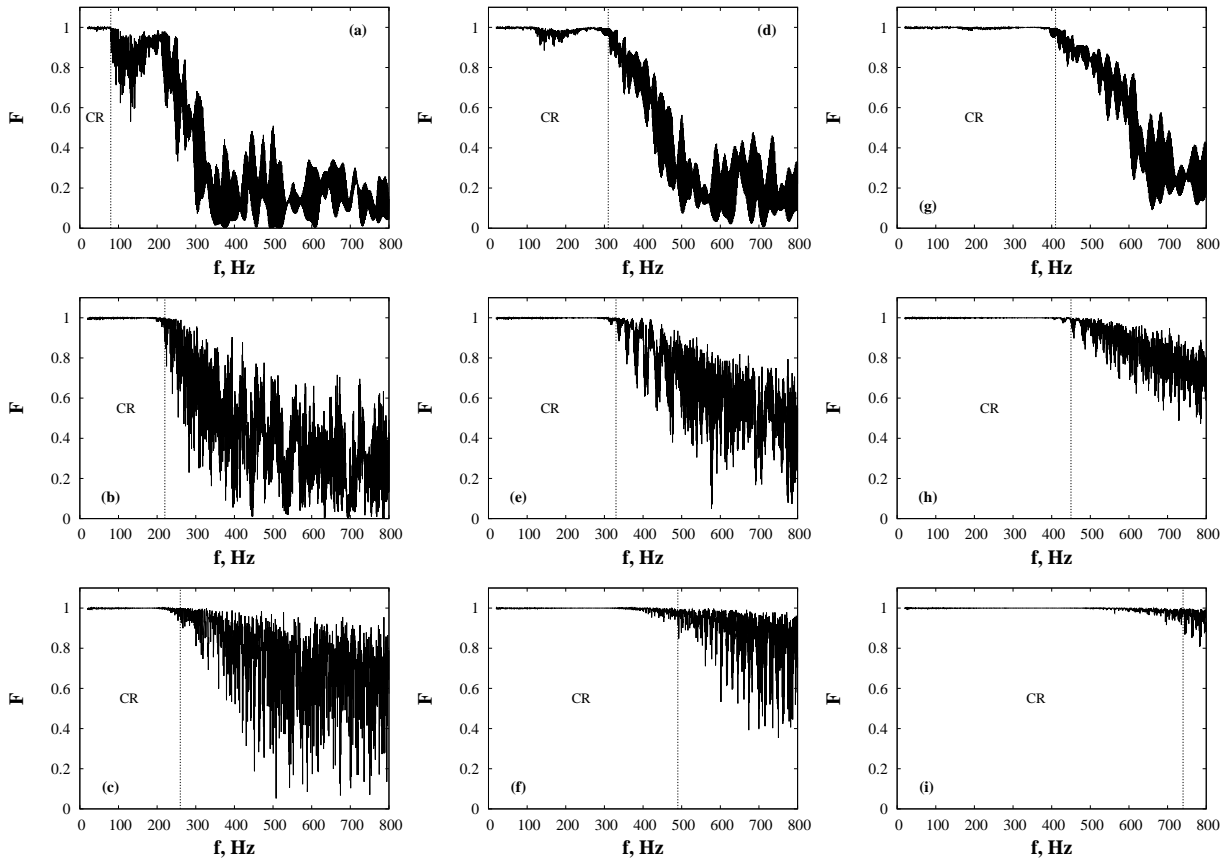


Fig. 4: Fidelity as the function of the signal frequency. The dashed line indicates the upper boundary of the confidence range (CR) in the frequency domain. Number of hydrophones in the array: 10 for panels (a)-(c), 15 for panels (d)-(f), and 20 for panels (g)-(i). Distance from the source: 1 km for the upper row of panels, 10 km for the middle row, and 40 km for the lower row.

130 into account that number of statistically independent transmissions might be limited in an actual experiment, we  
 131 conduct statistical analysis with relatively poor ensemble of ten realizations.

Reconstruction errors caused by ambient noise can be amplified by displacements of the array hydrophones from the depths determined by Eq. (17). Perturbation of similar kind was considered in [43]. Horizontal displacements can be reasonably considered as small compared with horizontal sound wavelength, therefore, their effect is negligible for the array performance. When constructing a model of such displacements, we can assume that the upper and lower ends of the array are tightly fixed at the surface and bottom, respectively. Then, the displacement field can be presented as sum of sine modes with random amplitudes. We restrict ourselves to the case of two modes, and the displacement profile is written as

$$\zeta(z) = \frac{\varsigma}{\sqrt{2}} \left( \zeta_1 \sin \frac{\pi z}{h} + \zeta_2 \sin \frac{2\pi z}{h} \right), \quad (36)$$

where  $\nu_1$  and  $\nu_2$  are statistically independent Gaussian random variables with zero mean and unit variance. In computations, r.m.s. amplitude of displacement  $\varsigma$  is taken 1 m. The resulting perturbation is a combination of

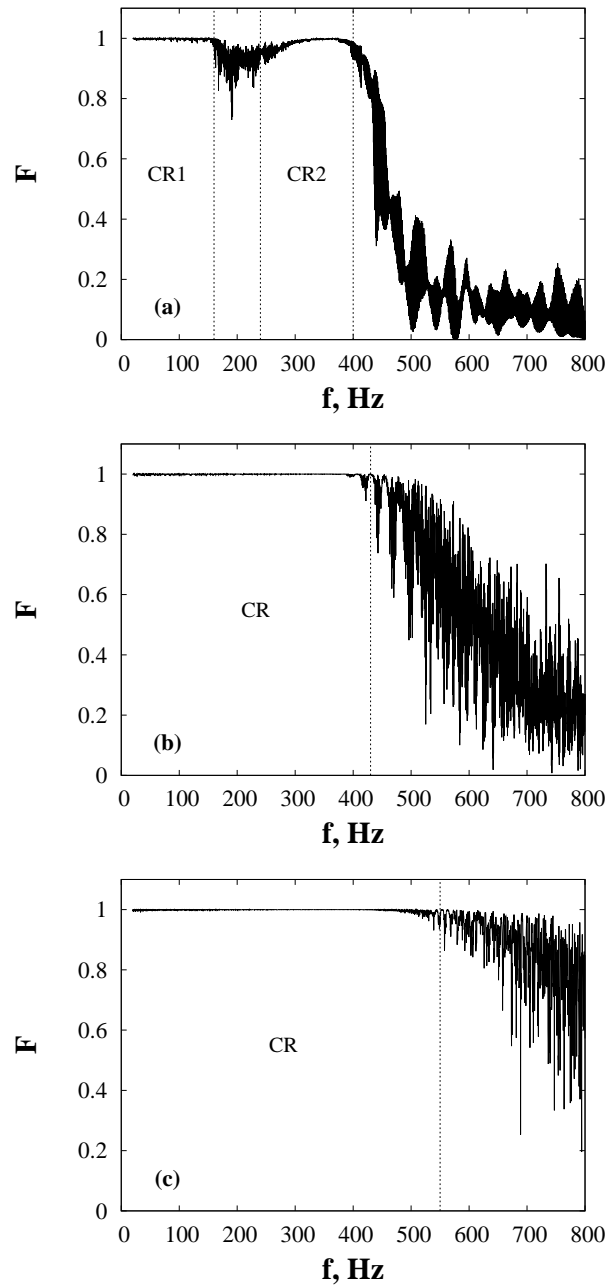


Fig. 5: The same as in Fig. 4(g)-(i), but for a source located at  $z = 1$  m. Two parts of the splitted confidence range in the case of  $r = 1$  km are denoted as “CR1” and “CR2”.

ambient noise and random hydrophone displacements, therefore Eq. (35) has the form

$$\Psi_{\text{measured}}(z_j) = \Psi(z_j + \zeta) + \xi_j, \quad (37)$$

Figure 6 demonstrates frequency dependence of fidelity for various values of signal-to-noise ratio (SNR). SNR is

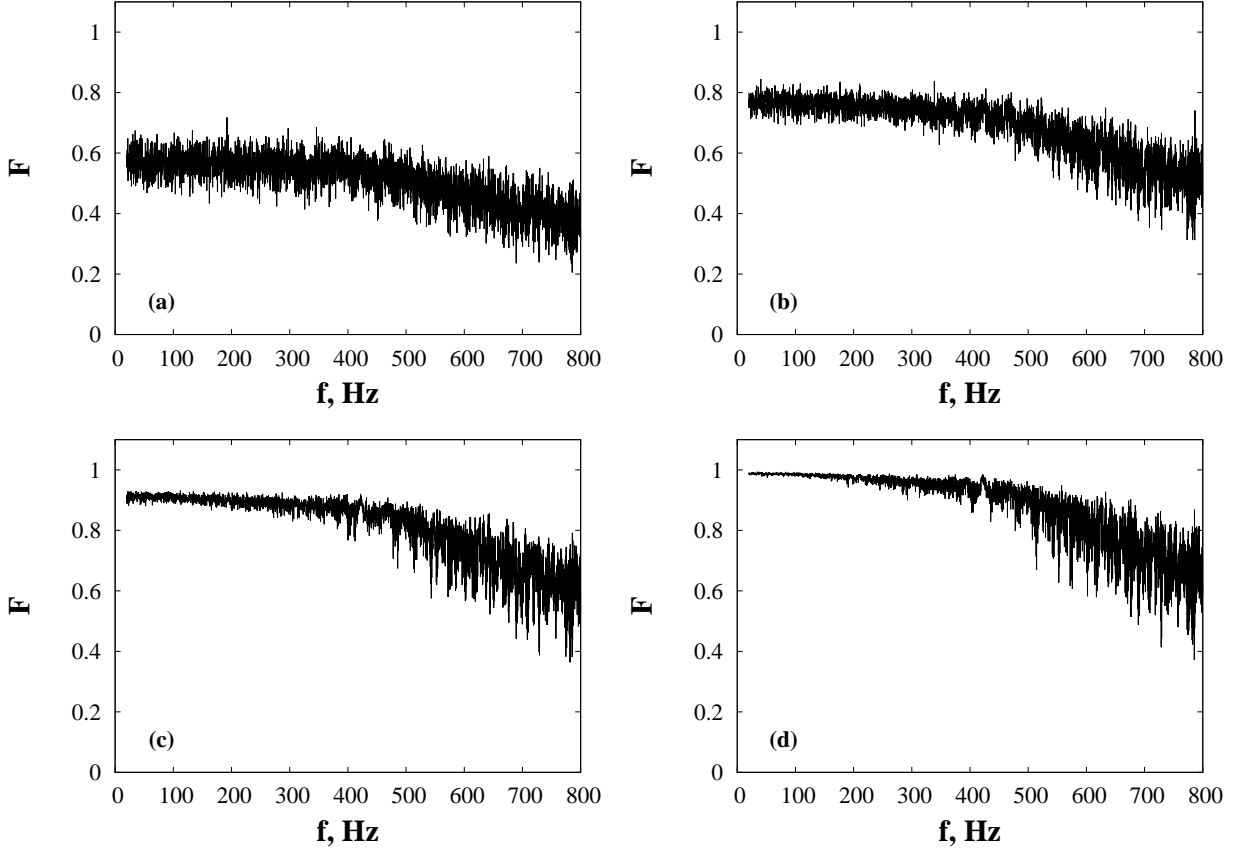


Fig. 6: Frequency dependence of fidelity averaged over 10 realizations of noise for the array with 20 hydrophones. (a)  $\text{SNR}_{\text{dB}} = 1$  dB, (b)  $\text{SNR}_{\text{dB}} = 5$  dB, (c)  $\text{SNR}_{\text{dB}} = 10$  dB, (d)  $\text{SNR}_{\text{dB}} = 20$  dB.

evaluated as

$$\text{SNR}_{\text{dB}} = 10 \log_{10} \frac{\left( \sum_{j=1}^J |\Psi_{\text{exact}}(z_j)|^2 \right)}{\sum_{j=1}^J |\xi_j|^2}, \quad (38)$$

where function  $\Psi_{\text{exact}}(z)$  is computed by Eq. (28). The data corresponds to the array with  $J = 20$  hydrophones and a point source located at  $z = 99$  m. Note that we simulate relatively difficult measurement conditions with low SNR values. It is found that the effect of displacements on the fidelity is weak as compared to that of the noise. Not surprisingly, the noise reduces accuracy of the reconstruction. Satisfactory level of the fidelity can be obtained with SNR of 10 dB or higher. However, influence of the noise can be significantly reduced by averaging measured values  $\tilde{\Psi}$  over realizations before inserting them into Eq. ((20)),

$$\langle \Psi \rangle (z_j) = \frac{1}{N} \sum_{n=1}^N \tilde{\Psi}(z_j). \quad (39)$$

132 Here  $N$  is number of realizations. Averaging substantially improves the quality of reconstruction, yielding accurate  
 133 reconstruction even in the case of  $\text{SNR} = 1$  dB (see Fig. 7).

134 Quality of reconstruction could be estimated by means of data presented in Figure 8. It illustrates the original  
 135 and reconstructed wavefield profiles in the same plot (the signal frequency in this case is 500 Hz). In this particular

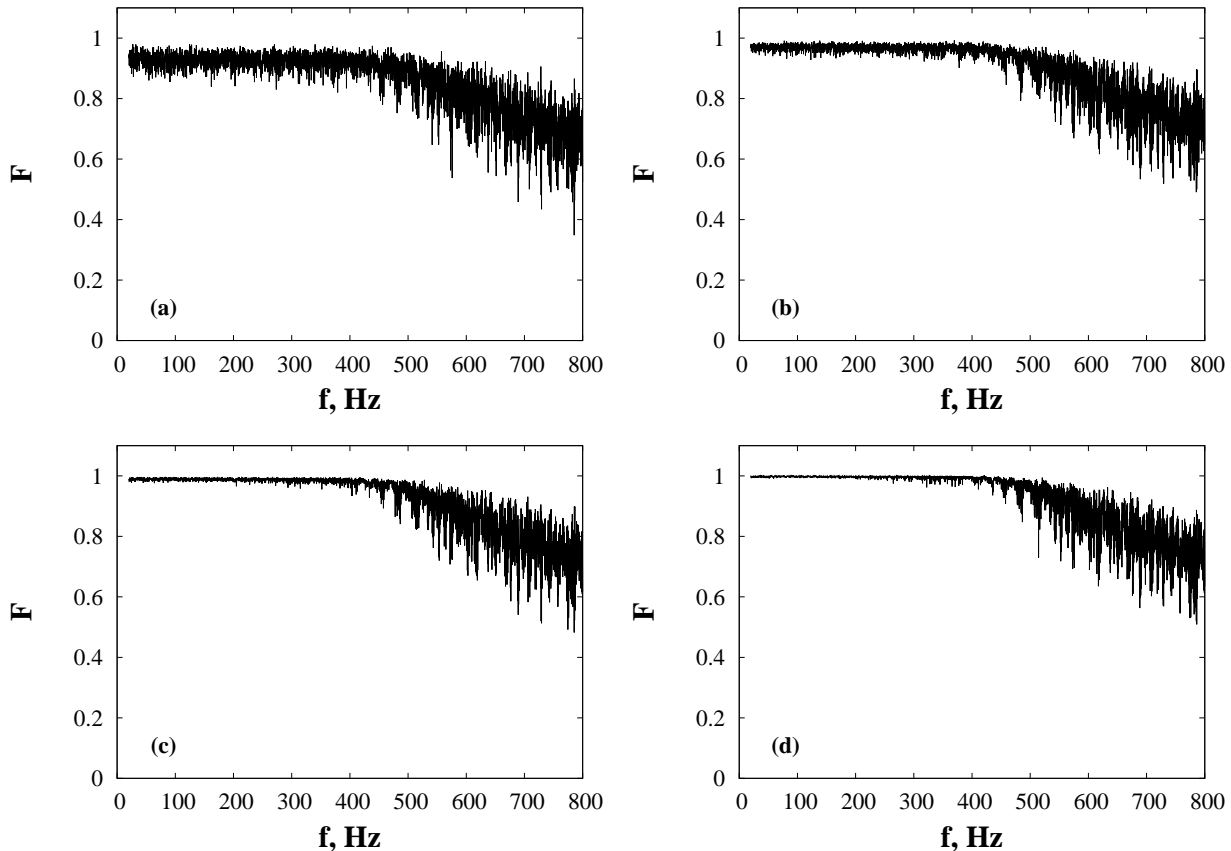


Fig. 7: Frequency dependence of fidelity calculated with the averaged data. The array consists of 20 hydrophones. (a)  $\text{SNR}_{\text{dB}} = 1$  dB, (b)  $\text{SNR}_{\text{dB}} = 5$  dB, (c)  $\text{SNR}_{\text{dB}} = 10$  dB, (d)  $\text{SNR}_{\text{dB}} = 20$  dB.

136 example, the fidelity value in the absence of fluctuations is 96.8%. We see that the profiles are very close to each  
 137 other, excepting the vicinity of  $z = 60$  m, where the reconstruction inaccurately reproduces form of an interference  
 138 peak.

139

#### IV. SELECTION OF THE SPACING BETWEEN HYDROPHONES

As it follows from Eq. (18), the array spacing  $\Delta z$  is determined by the total number of DVR functions  $j_{\text{max}}$ . For fixed depth of the sediment-basement interface  $L$ , its value can have a discrete set of values. In practice, however, accurate information about value  $L$  can be lacking. Furthermore, the low-order modes propagating predominantly inside the water column are almost insensitive to value of  $L$ , if the width of the sediment layer is sufficiently large. Consequently, if we are interested in sound propagation over distances of few kilometers, or more, when the wavefield is mainly formed by low-order modes, we have certain freedom in choosing  $L$ . It means that there are no strict limitations on the value of spacing  $\Delta z$ . For arbitrarily chosen value of  $\Delta z$ , we can replace the “actual” value of  $L$  by a fictitious one  $L'$  that is determined using the formula

$$L' = (j_{\text{max}} + 1)\Delta z. \tag{40}$$

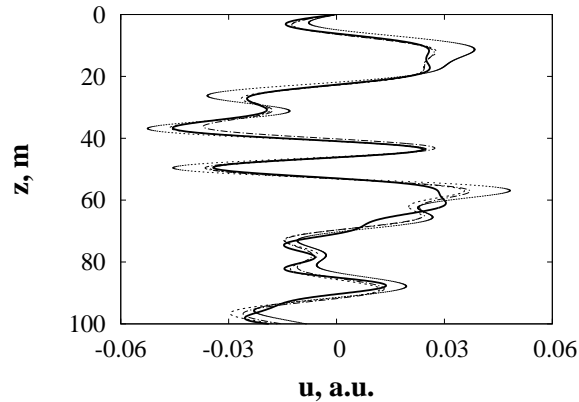


Fig. 8: Comparison of the original wavefield profile (bold solid line) with reconstructed ones. Dashed curve corresponds to reconstruction in the absence of fluctuations, fidelity  $F = 96.8\%$ . Dotted line corresponds to reconstruction for an individual realization of ambient noise with SNR 10 dB and array displacements with  $\zeta = 1$  m,  $F = 85.4\%$ . Dashed dotted line corresponds to reconstruction in the presence of fluctuations, with the preliminary averaging of a wavefield over 10 realizations,  $F = 94.9\%$ . The data corresponds to the array with 20 hydrophones. Signal frequency is 500 Hz. Propagation range is 10 km.

It leads to a slight modification of basis functions (6),

$$\phi_j = \sqrt{\frac{2}{L'}} \sin \frac{(2j-1)\pi z}{2L'}, \quad j = 1, 2, \dots \quad (41)$$

140 It should be noted that the value of  $j_{\max}$  has to be sufficiently large in order to eliminate the effect of the sediment-  
 141 basement interface onto structure of DVR functions inside the water column.

142 Thus, it turns out that the algorithm of wavefield reconstruction using the basis of DVR functions can be utilized  
 143 for any equally spaced vertical array, provided that the spacing is sufficient to reproduce vertical spectrum of a  
 144 wavefield. This property will be used in the next section for studying reconstruction of wavefields corresponding  
 145 to broadband signals.

146 V. RECONSTRUCTION OF PULSE WAVEFIELDS

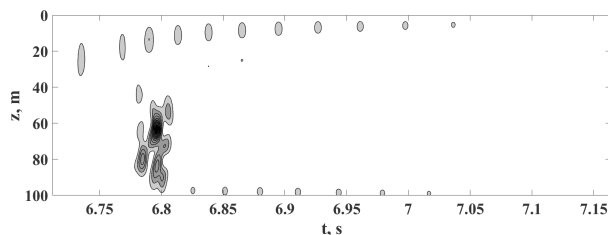


Fig. 9: A wavefield in the time-depth plane at range 10 km, the case of a broadband pulse with center frequency  $f_c = 240$  Hz. The pulse is created by a point source located near the bottom, at  $z = 99$  m.

Transient wavefield  $\tilde{u}$  corresponding to a sound pulse can be synthesized from cw wavefields  $u$  using the formula [37]

$$\tilde{\Psi}(t, z) = \int s(\Omega) \Psi(r, z, \Omega) e^{-i\Omega t} d\Omega, \quad (42)$$

where  $\Omega = 2\pi f$  is the angular frequency, and  $s(\Omega)$  is the spectrum of the signal emitted by the source. In our examples we consider broadband signals with the spectrum

$$s(\Omega) = \frac{T}{\sqrt{2\pi}} \exp\left[-\frac{(\Omega - \Omega_c)^2 T^2}{2}\right], \quad T = \frac{\sqrt{2\pi}}{\Delta\Omega}, \quad (43)$$

147 where  $\Delta\Omega = \Omega_c/2$ . Arrival pattern of such signal in the time-depth plane for the pulse with center frequency 240  
148 Hz is demonstrated in Fig. 9.

Fidelity for a pulse wavefield reconstruction can be defined in the same spirit as for cw wavefields, i. e.

$$F = \frac{1}{\tilde{A}_{\text{exact}} \tilde{A}_{\text{est}}} \int_{t=0}^{\infty} \int_{z=0}^h \tilde{\Psi}_{\text{exact}}^*(t, z) \tilde{\Psi}_{\text{est}}(t, z) dt dz \quad (44)$$

where the normalization factors are given by formulae

$$\tilde{A}_{\text{exact}} = \int_{t=0}^{\infty} \int_{z=0}^h |\tilde{\Psi}_{\text{exact}}(t, z)|^2 dt dz,$$

$$\tilde{A}_{\text{est}} = \int_{t=0}^{\infty} \int_{z=0}^h |\tilde{\Psi}_{\text{est}}(t, z)|^2 dt dz.$$

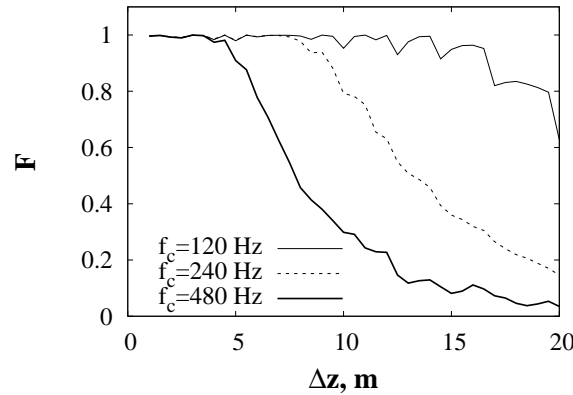


Fig. 10: Fidelity of a pulse wavefield vs array spacing for broadband pulses with different center frequencies.

149

150 Figure 10 shows fidelity decay with increasing of the array spacing  $\Delta z$  for pulses with center frequencies of 120,  
151 240 and 420 Hz. The pulses are emitted by the point source located near the bottom at  $z = 99$  m. As one would  
152 expect, the confidence range in the  $\Delta z$  space is inversely proportional to the pulse center frequency. Fidelity is  
153 nearly one within some limited interval of  $\Delta z$  that can be considered as the confidence range, and rapidly decreases  
154 outside it. Arrays with  $\Delta z \leq 4.5$  m provide almost exact reconstruction of all considered pulses.



## VI. CONCLUSION

In the present study we demonstrate a novel algorithm for the wavefield reconstruction relying upon the data collected by a vertical array of equally spaced hydrophones. The proposed algorithm can be considered a generalization of a Whittaker-Shannon interpolation procedure onto the case of underwater acoustic waveguides. Validity of the algorithm requires boundedness of wavefield Fourier spectrum. We see that sound attenuation in the bottom basically improves quality of reconstruction due to filtering of high-number modes. It implies that the fidelity dependencies presented in this paper are not universal and depend on the properties of a particular waveguide under consideration, as well as on the form of the transmitted signal.

The key idea of the algorithm is representation of a wavefield as expansion over DVR functions. The coefficients of the expansion are equal to acoustic wavefield values at an equispaced grid. It means that they can be measured using an equispaced vertical array, where each pointwise measurement contributes to the coefficient of only one DVR function in the expansion. It is very convenient from the viewpoint of error elimination: inaccuracies of data measured by different hydrophones do not interfere and can be processed separately. In the present paper we show that simple averaging over data from few transmissions is sufficient for substantial reduction of noise-induced inaccuracy. Such averaging can be very effective if noise correlation time is much smaller than the timescale of waveguide variability.

Another important advantage of the presented approach is the absence of explicit dependence of DVR functions on signal frequency. This feature makes it very well-suited for reconstruction of broadband pulses. Also, DVR functions do not depend on hydrological properties of a waveguide. It means that this approach can be readily implemented for analysis of data obtained by stationary systems of acoustic monitoring of marine environment variability.

Numerical simulations in this paper are conducted with a range-independent model of a waveguide. It would be interesting to examine effect of horizontal inhomogeneities onto accuracy of the proposed algorithm. For instance, it is reasonable to expect that sound scattering by random inhomogeneities should lead to additional pumping of high-number modes thereby reducing effect of their filtration. Another issue that should be addressed in future work is generalization of the algorithm to the case of arrays with variable spacing between receivers. In particular, in many cases it can be useful to decrease hydrophone spacing near the waveguide axis, where impact of shorter vertical wavelengths is more pronounced. Definitely, the feasibility of the wavefield reconstruction in a deep ocean propagation scenario also deserves investigation.

## ACKNOWLEDGMENT

This work was carried out in the framework of the POI FEB RAS Program “Mathematical simulation and analysis of dynamical processes in the ocean” (No. 0271-2019-0001).

## REFERENCES

- [1] J. R. Buck, J. C. Preisig, and K. E. Wage, “A unified framework for mode filtering and the maximum a posteriori mode filter,” *J. Acoust. Soc. Amer.*, vol. 103, no. 4, pp. 1813–1824, 1998. [Online]. Available: <https://doi.org/10.1121/1.421334>

- 190 [2] K. E. Wage, A. B. Baggeroer, and J. C. Preisig, "Modal analysis of broadband acoustic receptions at 3515-km range in the  
191 north pacific using short-time fourier techniques," *J. Acoust. Soc. Amer.*, vol. 113, no. 2, pp. 801–817, 2003. [Online]. Available:  
192 <https://doi.org/10.1121/1.1530615>
- 193 [3] K. E. Wage, M. A. Dzieciuch, P. F. Worcester, B. M. Howe, and J. A. Mercer, "Mode coherence at megameter ranges in the North Pacific  
194 Ocean," *J. Acoust. Soc. Am.*, vol. 117, no. 3, pp. 1565–1581, 2005.
- 195 [4] A. K. Morozov, J. C. Preisig, and J. C. Papp, "Investigation of mode filtering as a preprocessing method for shallow-water acoustic  
196 communications," *IEEE J. Ocean. Engin.*, vol. 35, no. 4, pp. 744–755, 2010.
- 197 [5] M. Labutina, A. Malekhanov, and A. Smirnov, "Estimation of efficiency of vertical antenna arrays in underwater sound channels," *Phys.*  
198 *Wave Phenom.*, vol. 24, no. 2, pp. 161–167, 2016.
- 199 [6] F. J. Beron-Vera, M. G. Brown, J. A. Colosi, S. Tomsovic, A. L. Virovlyansky, M. A. Wolfson, and G. M. Zaslavsky, "Ray dynamics in  
200 a long-range acoustic propagation experiment," *J. Acoust. Soc. Am.*, vol. 114, no. 3, pp. 1226–1242, 2003.
- 201 [7] P. Artel'nyi, A. Virovlyansky, A. Kazarova, P. Korotin, L. Lyubavin, and A. Stulenkov, "Observation of stable sound field components in  
202 lake ladoga," *Acoust. Phys.*, vol. 64, no. 2, pp. 175–185, 2018.
- 203 [8] E. C. Shang, "Ocean acoustic tomography based on adiabatic mode theory," *J. Acoust. Soc. Am.*, vol. 85, no. 4, pp. 1531–1537, 1989.
- 204 [9] E. Gorodetskaya, A. Malekhanov, and V. Talanov, "Simulation of processing of optimal array signal in underwater sound channels,"  
205 *Akusticheskij Zhurnal*, vol. 38, no. 6, pp. 1044–1051, 1992.
- 206 [10] R. M. Jones, E. C. Shang, and T. M. Georges, "Nonperturbative modal tomography inversion. Part I. Theory," *J. Acoust. Soc. Am.*, vol. 94,  
207 no. 4, pp. 2296–2302, 1993.
- 208 [11] D. V. Makarov, L. E. Kon'kov, and P. S. Petrov, "Influence of oceanic synoptic eddies on duration of modal acoustic pulses," *Radiophys.*  
209 *Quant. Electron.*, vol. 58, no. 12, pp. 1–15, 2016.
- 210 [12] L. Dumaz, J. Garnier, and G. Lepoutlier, "Acoustic and geoacoustic inverse problems in randomly perturbed shallow-water environments,"  
211 *J. Acoust. Soc. Am.*, vol. 146, no. 1, pp. 458–469, 2019.
- 212 [13] A. Rutenko, V. Gritsenko, D. Kovzel, D. Manulchev, and M. Fershalov, "A method for estimating the characteristics of acoustic pulses  
213 recorded on the Sakhalin shelf for multivariate analysis of their effect on the behavior of gray whales," *Acoust. Phys.*, vol. 65, no. 5, pp.  
214 556–566, 2019.
- 215 [14] S. H. Abadi and E. Freneau, "Short-range propagation characteristics of airgun pulses during marine seismic reflection surveys," *J. Acoust.*  
216 *Soc. Am.*, vol. 146, no. 4, pp. 2430–2442, 2019.
- 217 [15] Y. Lu, K. Yang, and R. Duan, "A simple method for depth estimation of a sound source at known range in the deep sea," *J. Acoust. Soc.*  
218 *Am.*, vol. 146, no. 6, pp. 4097–4107, 2019.
- 219 [16] A. L. Virovlyansky, A. Y. Kazarova, and L. Y. Lyubavin, "Matched field processing in phase space," *IEEE J. Ocean. Engin.*, pp. 1–11,  
220 2019.
- 221 [17] W. Liu, Y. Yang, L. Lü, Y. Shi, and Z. Liu, "Source localization by matching sound intensity with a vertical array in the deep ocean," *J.*  
222 *Acoust. Soc. Am.*, vol. 146, no. 6, pp. EL477–EL481, 2019. [Online]. Available: <https://doi.org/10.1121/1.5139191>
- 223 [18] M. Volkov, V. Grigoriev, A. Lunkov, and V. Petnikov, "On the possibility of using vertical receiving arrays for underwater acoustic  
224 communication on the arctic shelf," *Acoust. Phys.*, vol. 65, no. 3, pp. 269–278, 2019.
- 225 [19] A. A. Lunkov, "Interference structure of low-frequency reverberation signals in shallow water," *Acoust. Phys.*, vol. 61, no. 5, pp. 547–555,  
226 Sep 2015.
- 227 [20] A. Lunkov, "Spatio-temporal variability of bottom reverberation striation pattern in shallow water," *J. Acoust. Soc. Am.*, vol. 141, no. 5,  
228 pp. 4005–4005, 2017.
- 229 [21] K. C. Hegewisch, N. R. Cerruti, and S. Tomsovic, "Ocean acoustic wave propagation and ray method correspondence: Internal wave fine  
230 structure," *J. Acoust. Soc. Am.*, vol. 117, no. 3, pp. 1582–1594, 2005.
- 231 [22] I. A. Udovydchenkov and M. G. Brown, "Modal group time spreads in weakly range-dependent deep ocean environments," *J. Acoust. Soc.*  
232 *Am.*, vol. 123, no. 1, pp. 41–50, 2008.
- 233 [23] A. K. Morozov and J. A. Colosi, "Entropy and scintillation analysis of acoustical beam propagation through ocean internal waves," *J.*  
234 *Acoust. Soc. Am.*, vol. 117, no. 3, pp. 1611–1623, 2005.
- 235 [24] J. A. Colosi and A. K. Morozov, "Statistics of normal mode amplitudes in an ocean with random sound-speed perturbations: Cross-mode  
236 coherence and mean intensity," *J. Acoust. Soc. Am.*, vol. 126, no. 3, pp. 1026–1035, 2009.
- 237 [25] J. A. Colosi, T. F. Duda, and A. K. Morozov, "Statistics of low-frequency normal-mode amplitudes in an ocean with random sound-speed  
238 perturbations: Shallow-water environments," *J. Acoust. Soc. Am.*, vol. 131, no. 2, pp. 1749–1761, 2012.

- 239 [26] I. A. Udovychenkov, M. G. Brown, T. F. Duda, J. A. Mercer, R. K. Andrew, P. F. Worcester, M. A. Dzieciuch, B. M. Howe, and J. A.  
240 Colosi, “Modal analysis of the range evolution of broadband wavefields in the north pacific ocean: Low mode numbers,” *J. Acoust. Soc.*  
241 *Am.*, vol. 131, no. 6, pp. 4409–4427, 2012.
- 242 [27] S. Abdullaev and G. Zaslavskii, “Classical nonlinear dynamics and chaos of rays in problems of wave propagation in inhomogeneous  
243 media,” *Sov. Phys. Usp.*, vol. 34, no. 8, pp. 645–664, 1991.
- 244 [28] M. G. Brown, J. A. Colosi, S. Tomsovic, A. L. Virovlyansky, M. A. Wolfson, and G. M. Zaslavsky, “Ray dynamics in long-range deep  
245 ocean sound propagation,” *J. Acoust. Soc. Am.*, vol. 113, no. 5, pp. 2533–2547, 2003.
- 246 [29] D. Makarov, S. Prants, A. Virovlyansky, and G. Zaslavsky, *Ray and wave chaos in ocean acoustics: chaos in waveguides*, ser. Series on  
247 complexity, nonlinearity and chaos. Singapore: World Scientific, 2010.
- 248 [30] A. L. Virovlyansky, D. V. Makarov, and S. V. Prants, “Ray and wave chaos in underwater acoustic waveguides,” *Phys. Usp.*, vol. 55, no. 1,  
249 pp. 18–46, 2012.
- 250 [31] D. V. Makarov, L. E. Kon’kov, M. Yu. Uleysky, and P. S. Petrov, “Wave chaos in a randomly inhomogeneous waveguide: spectral analysis  
251 of the finite-range evolution operator,” *Phys. Rev. E*, vol. 87, p. 012911, Jan 2013.
- 252 [32] D. Makarov, “Random matrix theory for low-frequency sound propagation in the ocean: A spectral statistics test,” *J. Theor. Comput.*  
253 *Acoust.*, vol. 26, p. 1850002, 2018.
- 254 [33] M. Beck, A. Jäckle, G. Worth, and H.-D. Meyer, “The multiconfiguration time-dependent hartree (mctdh) method: a highly efficient  
255 algorithm for propagating wavepackets,” *Phys. Rep.*, vol. 324, no. 1, pp. 1 – 105, 2000.
- 256 [34] G. A. Pitsevich and A. E. Malevich, “Comparison of the fourier and discrete-variable-representation methods in the numerical solution of  
257 multidimensional schrödinger equations,” *J. Appl. Spectrosc.*, vol. 82, no. 6, pp. 893–900, Jan 2016.
- 258 [35] S. Paul and E. Tiesinga, “Wannier functions using a discrete variable representation for optical lattices,” *Phys. Rev. A*, vol. 94, p. 033606,  
259 Sep 2016.
- 260 [36] J. Duron, M. Beauregard, I. De La Cruz, M. Knodell, R. Cardenas, and R. Lombardini, “Computation of the exciton ground state in  
261 arbitrarily shaped quantum dots using discrete variable representation method,” *J. Comput. Theor. Nanosci.*, vol. 14, no. 4, pp. 1706–1713,  
262 2017.
- 263 [37] F. B. Jensen, W. A. Kuperman, M. B. Porter, and H. Schmidt, *Computational ocean acoustics*. Springer Science & Business Media,  
264 2011.
- 265 [38] D. V. Makarov, M. Yu. Uleysky, and S. V. Prants, “Ray chaos and ray clustering in an ocean waveguide,” *Chaos*, vol. 14, pp. 79–95, 2004.
- 266 [39] D. V. Makarov and M. Yu. Uleyskiy, “Ray escape from a range-dependent underwater sound channel,” *Acoust. Phys.*, vol. 53, no. 4, pp.  
267 495–502, 2007.
- 268 [40] J.-X. Zhou, X.-Z. Zhang, and D. P. Knobles, “Low-frequency geoacoustic model for the effective properties of sandy seabottoms,” *J.*  
269 *Acoust. Soc. Am.*, vol. 125, no. 5, pp. 2847–2866, 2009.
- 270 [41] P. S. Petrov. (2019) ac\_modes: simple matlab code for the computation of acoustical normal modes in the ocean. [Online]. Available:  
271 [https://github.com/kaustikos/ac\\_modes](https://github.com/kaustikos/ac_modes)
- 272 [42] D. Makarov, “On measurement of acoustic pulse arrival angles using a vertical array,” *Acoust. Phys.*, vol. 63, no. 6, pp. 673–680, 2017.
- 273 [43] V. A. Eliseevnin and Y. I. Tuzhilkin, “The directivity of a radiating line array slightly deflected from vertical in a waveguide,” *Acoust.*  
274 *Phys.*, vol. 48, no. 5, pp. 552–557, 2002.

275 **Denis Makarov** D. Makarov graduated from Krasnoyarsk State University in 1999 (diploma in physics). After the university he joined V.I.II’ichev  
276 Pacific Oceanological Institute (POI), the Laboratory of Nonlinear Dynamical Systems, as a Ph.D. student. He received Ph.D. degree in acoustics  
277 in 2004 and became a senior researcher of POI. In 2015, he received Dr.Sci. degree in theoretical physics and was promoted to leading research  
278 associate of POI. Denis Makarov won several awards and prizes, including medal of the Russian Academy of Sciences for young scientists,  
279 L.M. Brekhovskikh medal from the Russian Acoustical Society, V.I.II’ichev and U.H.Kopvillem awards from the Far-Eastern Branch of the  
280 Russian Academy of Sciences, and stipend of the Dynasty Foundation. The main fields of his research are underwater acoustics, chaos theory,  
281 quantum optics, and ultracold atoms.

282 **Pavel Petrov** P. Petrov graduated from Irkutsk State University in 2006 (diploma in pure mathematics with distinction). In the same year he  
283 joined V.I.II'ichev Pacific Oceanological Institute (POI) as a Ph.D. student. He received his Ph.D. degree in theoretical physics in 2010 and  
284 continued his work at POI as a senior researcher. In 2019 he became head of laboratory of Geophysical Hydrodynamics. In parallel, P. Petrov  
285 also taught mathematics (algebra, group theory, computer algebra, calculus) at Far Eastern Federal University starting as teaching assistant  
286 (2007) and later being promoted to assistant professor (2009) and associate professor (2010).

287 P. Petrov had several scholarships at leading Russian research institutions, including St. Petersburg Department of Steklov Mathematical  
288 Institute and Institute for Problems in Mechanics (Moscow). He also had a postdoc scholarship in acoustics at University of Haifa (Israel), three  
289 scholarships in applied mathematics at University of Wuppertal (Germany) and a scholarship at University of Lorraine (France).

290 His research interests include mathematical physics, computational underwater acoustics, geoacoustic inversion, semi-analytical methods for  
291 3D sound propagation.